Advances in Applied Mathematics and Mechanics
Adv. Appl. Math. Mech., Vol. **16**, No. 2, pp. 331-354

DOI: 10.4208/aamm.OA-2022-0303
April 2024

Numerical Computation of Helical Waves in a Finite Circular Cylinder using Chebyshev Spectral Method

Xing-Liang Lyu and Wei-Dong Su*

State Key Laboratory for Turbulence and Complex Systems and Department of Mechanics and Engineering Science, College of Engineering, Peking University, Beijing 100871, China

Received 19 November 2022; Accepted (in revised version) 9 March 2023

Abstract. Helical waves are eigenfunctions of the curl operator and can be used to decompose an arbitrary three-dimensional vector field orthogonally. In turbulence study, high accuracy for helical waves especially of high wavenumber is required. Due to the difficulty in analytical formulation, the more feasible strategy to obtain helical waves is numerical computation. For circular cylinders of finite length, a semi-analytical method via infinite series to formulate the helical wave is known [E. C. Morse, J. Math. Phys., 46 (2005), 113511], where the eigenvalues are evaluated by iterating transcend equations. In this paper, the numerical computation for helical wave in a finite circular cylinder is implemented using a Chebyshev spectral method. The solving is transformed into a standard matrix eigenvalue problem. The large eigenvalues are computed with high precision, and the calculation cost to rule out spurious eigenvalues is significantly reduced with a new criterion suggested.

AMS subject classifications: 65N25, 65N35, 76F02, 76W05

Key words: Helical wave, Chandrasekhar-Kendall mode, eigenvalue problem, Chebyshev spectral method, spurious eigenvalues, circular cylinder.

1 Introduction

1.1 Background

Helical waves are the eigenfunctions of the curl operator, which was first noted by Beltrami [1]. It is also called force-free fields [2] in physics, or Taylor state [3] associating with a variational principle, and helical Fourier modes [4,5]. The terminology of "helical wave" has been introduced by Moffatt [6]. They have been widely used in fluid dynamics and magnetohydrodynamics. Yoshida and Giga [7] proved that helical waves can span a

*Corresponding author.
Email: swd@pku.edu.cn (W.-D. Su)

 ©2024 Global Science Press

complete Hilbert space for solenoidal vector fields under proper boundary conditions in bounded domains of three-dimensional (3-D) space, and the corresponding helical wave decomposition (HWD) has been employed to analyze the global energy spectrum of turbulence in several cases [8]. In particular, the spectral coefficients of helical waves are scalars, and HWD can be taken as the generalization of Fourier basis functions in general bounded domains.

HWD plays an essential role in studying the energy cascade of homogeneous turbulence. Waleffe [9] investigated the nonlinear energy transfer of homogeneous turbulence and found that the scale and polarities of helical modes affect the direction of energy transfer. Chen et al [10] proved that the nonlinear transfer between opposite polarities permits the joint cascade of energy and helicity. Biferale et al [11] showed that an inverse energy cascade also occurs in 3-D isotropic turbulence by keeping only triadic interactions between sign-defined helical modes. And they also investigated the transfer properties of energy and helicity fluctuations by keeping only those triads that have sign-definite helicity content [12]. Helical waves are also used to study the decoupling mechanism between two-dimensional (2-D) modes and 3-D modes in rotating homogeneous turbulence [13,14].

For magnetic fields, helical modes play an essential role in the coupling mechanism between the external helicity source and the driven plasma [15,16]. Due to its completeness as functional basis, HWD are also be used for hydrodynamics simulations using Galerkin spectral representation [17–21], or helicity calculation [22]. In addition, helical waves can also be used to construct vortex knots [23]. An early standard reference to introduce the interdisciplinary application of helical waves comes from Moses [24].

Helical waves in an arbitrary bounded and simply connected domain $\mathcal{D}$ are solutions of the eigenfunction equation

$$\nabla\times\boldsymbol{B}=k\boldsymbol{B} \tag{1.1}$$

with the homogeneous boundary condition

$$\boldsymbol{B}\cdot\boldsymbol{n}|_{\partial\mathcal{D}}=0, \tag{1.2}$$

where $\boldsymbol{B}$ denotes helical wave and k denotes eigenvalue. As proved by Yoshida and Giga [7], an arbitrary solenoidal field in 3-D space can be decomposed into a series of orthogonal helical waves. This is the basis for the multi-scale expansion of vector fields, which can naturally be applied to turbulence studies.

Taking the curl of Eq. (1.1) again yields

$$\nabla^2\boldsymbol{B}+k^2\boldsymbol{B}=\boldsymbol{0}, \tag{1.3}$$

which is the Helmholtz equation that looks more familiar. However, Eq. (1.3) is just a necessary but insufficient condition for Eq. (1.1) to be satisfied. The case of $k=0$ is the well-known potential field, thus only nonzero eigenvalue k is concerned in the study.

For some simple geometries, such as a periodic box [24] and spherically symmetric domains [25], helical waves can be constructed directly or solved by Eq. (1.1) analytically under the boundary condition imposed on as Eq. (1.2). It is by no means an easy task to solve the eigenvalue problem for other domains.

To make the solving of helical wave be more feasible, some additional features of the helical wave should be explored. According to Chandrasekhar and Kendall [26], the vector field $\boldsymbol{B}$ can also be expressed by a scalar generating function

$$\boldsymbol{B}=k\nabla\times(\psi\boldsymbol{a})+\nabla\times\nabla\times(\psi\boldsymbol{a}) \tag{1.4}$$

with a fixed unit vector $\boldsymbol{a}$ in space. And ψ is a solution of the scalar Helmholtz equation

$$\nabla^2\psi+k^2\psi=0. \tag{1.5}$$

Obviously, the boundary condition satisfied by Eq. (1.5) becomes more complicated than the ordinary due to the non-penetration of $\boldsymbol{B}$ on the boundary of the domain along with the unconventional form of Eq. (1.4). Despite the peculiarity, the scalar Helmholtz equation is easier to be handled than Eq. (1.1) which is actually a set of coupling equations. Indeed, using the separation of variable analysis, the eigenfunctions after the name of Chandrasekhar-Kendall (CK) modes can be obtained for the cases of periodic cylinder [17], sphere [19], specific types of spheromaks [27], finite cylinder [28], annular geometry [29], and periodic channel [30]. Specifically, Alkauskas [31] constructed two unique Beltrami vector fields with orientation-preserving icosahedral symmetry. For general domains, there are generally no analytical solutions for CK modes, and hence numerical solutions are necessary for finding the helical waves. We would like to emphasize that the investigation of all of the helical waves in the mentioned domains of various geometry are welcome due to their fundamental explicit or underlying applications in fluid dynamics, plasma physics or astrophysics, and etc.

Boulmezaoud and Amari [32] solved helical waves through an iteration approximation based on the finite element method. The algorithm can be applied to arbitrary bounded 3-D domain but the numerical precision is limited. On another line, Tang [33] emphasized the importance of non-axisymmetric modes and proposed a new formulation for numerically computing helical waves: the primitive Eq. (1.1) can be transformed into a standard matrix eigenvalue problem. By a second order finite difference scheme, Tang illustratively evaluated helical wave of some low wavenumber in an axisymmetric torus domain and also carried out the validation test.

In this paper, we numerically solved the helical wave in a circular cylinder domain of finite length following the formulation of [33] but the discretization strategy is different. We employ a Chebyshev spectral method which is capable of reaching high accuracy due to the spectral discretization nature. To our best knowledge, there was no similar work on solving helical wave by using a spectral method previously. Furthermore, a new criterion to rule out spurious eigenvalues during computation is proposed. As the necessary comparison to our method, the semi-analytical method proposed by Morse [28] will be

introduced briefly in advance in the next subsection. Also, a problem on eigenvalue evaluation in the semi-analytical method in [28] is found and corrected wherein.

1.2 Semi-analytical solution of helical wave in a finite cylinder

For the case of a finite cylinder, the separation of variable method can be used to find the axisymmetric helical waves (modes) due to the symmetry of the domain. Thus this is not our concern but mention that the axisymmetric modes are first solved by Finn [34]. The same analytical method cannot be used any longer for non-axisymmetric modes since the radial and axial variables are coupled wherein. Morse [28] has found the non-axisymmetric CK modes represented by series solution in terms of radial Bessel functions. By cylindrical coordinates, the scalar function can be written as

$$\psi(r,\theta,z)=e^{-im\theta}(F(r,z)+iG(r,z)), \tag{1.6}$$

where $F(r,z)$ and $G(r,z)$ are real functions since the range of z is shifted to $[-1/2,1/2]$, assuming the height and the radius of the cylinder are one unit and R_0 respectively. The radial boundary conditions with boundaries $r=R_0$ and $z=\pm 1/2$ imply that

$$\left(\frac{R_0}{mk}\right)\frac{\partial^2 G(r,z)}{\partial r\partial z}\bigg|_{r=R_0}=-F(R_0,z), \tag{1.7a}$$

$$\left(\frac{R_0}{mk}\right)\frac{\partial^2 F(r,z)}{\partial r\partial z}\bigg|_{r=R_0}=G(R_0,z). \tag{1.7b}$$

Using the separable solutions to the scalar Helmholtz equation, the general series expression for ψ is

$$\begin{aligned}\psi(r,z)e^{im\theta}=&-\frac{1}{2|m|}\cdot r^{|m|}\cdot e^{ikz}+\sum_{n'=1}^{\infty}b_{n'}\frac{J_m(\sqrt{k^2-((2n'-1)\pi)^2}\cdot r)}{J_m(\sqrt{k^2-((2n'-1)\pi)^2}\cdot R_0)}\cdot\cos\big((2n'-1)\pi z\big)\\&+i\sum_{n=1}^{\infty}a_n\frac{J_m(\sqrt{k^2-(2n\pi)^2}\cdot r)}{J_m(\sqrt{k^2-(2n\pi)^2}\cdot R_0)}\cdot\sin(2n\pi z),\end{aligned} \tag{1.8}$$

where the Bessel function becomes imaginary at negative variables. Substituting Eq. (1.8) into Eq. (1.7), a set of matrix equations can be formed via series mapping

$$Z^{\text{even}}\cdot a=u_1', \tag{1.9a}$$

$$Z^{odd}\cdot b=u_2', \tag{1.9b}$$

where Z^{even} and Z^{odd} are decoupled mapping matrices, u_1' and u_2' are vectors containing the mapping matrix element, a and b are vectors containing the coefficients a_n and b_n, respectively. Then, by integration respect to radial boundary condition the eigenvalue equation can be derived as

$$\varepsilon(k)=\sum_{n'=1}^{\infty}\frac{b_{n'}(-1)^{n'}}{(2n'-1)}+\left(\frac{1}{2m}+\frac{1}{2|m|}\right)\cdot\pi R_0{}^{|m|}\frac{\sin(k/2)}{k}=0. \tag{1.10}$$

It is important to note that there is a bug in that equation in the original literature. Here the correct equation is presented. The eigenvalue k is then located by solving $\varepsilon(k)$ with finite terms of the series of b_n using the mapping matrix solution. Newton-Raphson method and bisection method are employed to find the roots of Eq. (1.10). The advantage of this method is that the eigenvalues have high accuracy. However, the scan interval of $\varepsilon(k)$ should be pretty small to ensure that no eigenvalues are missed. Thus, the calculation cost is very high. More importantly, though, the nearby interval of the integral multiple of π needs to be skipped for high m modes because Bessel function at small variable with high m modes is smaller than the machine precision 10^{-308}. For example, the value of modified Bessel function $I_{60}\left(10^{-4}\right)$ is 1.04×10^{-340} and $I_{280}\left(10^{-4}\right)$ is even 3.07×10^{-1770}. As a consequence, the completeness of helical waves of higher order modes is lost in double precision calculation if using Morse's method.

It is not clear how to discretize the Chandrasekhar-Kendall scalar function into a standard matrix eigenvalue problem with second order boundary condition, as discussed by Tang [33].

2 Numerical methods

2.1 Formation of matrix eigenvalue problem with regularity condition

For an axisymmetric domain, the helical modes $\boldsymbol{B}=B_r\hat{\mathbf{r}}+B_\theta\widehat{\boldsymbol{\theta}}+B_z\hat{\mathbf{z}}$ can be written as the following Fourier mode

$$B^m_{r,\theta,z}=b^m_{r,\theta,z}(r,z)e^{im\theta}. \tag{2.1}$$

Since the linear superposition of all the modes $\boldsymbol{B}$ represents a real vector field, we have

$$b^{-m}_{r,\theta,z}(r,z)={b^m_{r,\theta,z}}^*(r,z), \tag{2.2}$$

where the asterisk as the superscript denotes complex conjugate. In the following, $b^m_{r,\theta,z}(r,z)$ is denoted as $b_{r,\theta,z}(r,z)$ for simplicity. Substituting Eq. (2.1) into Eq. (1.1), one finds

$$\frac{im}{r}b_z-\frac{\partial b_\theta}{\partial z}=kb_r, \tag{2.3a}$$

$$\frac{\partial b_r}{\partial z}-\frac{\partial b_z}{\partial r}=kb_\theta, \tag{2.3b}$$

$$\frac{1}{r}\frac{\partial}{\partial r}(rb_\theta)-\frac{im}{r}b_r=kb_z. \tag{2.3c}$$

This set of equations can be discretized on a numerical grid, giving rise to a standard matrix eigenvalue problem. However, it should be noted that the helical mode calculation is severely polluted by spurious solutions because the constraint $\nabla\cdot\boldsymbol{B}=0$ is implicitly imposed, as indicated by Tang [33].

An alternatively formulation [33] was used to yield a standard matrix eigenvalue problem of the general form, which explicitly ensures the divergence-free condition. The incompressible condition of $\boldsymbol{B}$ is

$$\frac{1}{r}\frac{\partial}{\partial r}(rb_r)+\frac{1}{r}imb_\theta+\frac{\partial b_z}{\partial z}=0. \tag{2.4}$$

This can then be rewritten as

$$b_\theta=\frac{i}{m}\left(\frac{\partial}{\partial r}(rb_r)+r\frac{\partial b_z}{\partial z}\right). \tag{2.5}$$

Substituting Eq. (2.5) into Eq. (2.3a) and Eq. (2.3c), we have

$$-\frac{i}{m}r\frac{\partial}{\partial r}\frac{\partial}{\partial z}b_r-\frac{i}{m}\frac{\partial}{\partial z}b_r-\frac{i}{m}r\frac{\partial^2}{\partial z^2}b_z+\frac{im}{r}b_z=k\cdot b_r, \tag{2.6a}$$

$$\frac{ir}{m}\frac{\partial^2}{\partial r^2}b_r+\frac{3i}{m}\frac{\partial}{\partial r}b_r+\left(\frac{i}{mr}-\frac{im}{r}\right)b_r+\frac{2i}{m}\frac{\partial}{\partial z}b_z+\frac{i}{m}r\frac{\partial}{\partial r}\frac{\partial}{\partial z}b_z=k\cdot b_z. \tag{2.6b}$$

After proper discretization, the above equations form the standard matrix eigenvalue problem again. Taking into account the homogeneous boundary conditions for b_r and b_z on the surface of the cylinder, the whole problem will kept such nature. However, the natural boundary conditions on the axis need to be determined. Let us continue to proceed the regularity problem.

The normal non-penetration conditions $\boldsymbol{B}\cdot\boldsymbol{n}=0$ on boundaries $r=R_0$ and $z=\pm\frac{1}{2}$ imply

$$b_r|_{r=R_0}=b_z|_{z=-\frac{1}{2}}=b_z|_{z=-\frac{1}{2}}=0. \tag{2.7}$$

Inside the cylinder, the regularity conditions at the axis $r=0$ are needed. For b_z, taking the limit $r\to 0$ of Eq. (2.6a) and considering the regularities of all of the derivatives, one obtains

$$-\frac{i}{m}\frac{\partial}{\partial z}b_r+\frac{im}{r}b_z=k\cdot b_r. \tag{2.8}$$

Since $-\frac{i}{m}\frac{\partial}{\partial z}b_r$ and $k\cdot b_r$ are both finite as well as $m\neq 0$, so

$$\lim_{r\to 0}\frac{b_z}{r}=C, \tag{2.9}$$

where C means a constant. Hence, we have homogeneous Dirichlet condition

$$\lim_{r\to 0}b_z=0. \tag{2.10}$$

For b_r, the limit $r\to 0$ of Eq. (2.6b) gives the results that are different for $m=1$ and $m>1$. For $m>1$ the regularity condition of b_r which reads

$$\lim_{r\to 0}\left(\frac{i}{m}-im\right)b_r=0 \tag{2.11}$$

implies

$$\lim_{r\to 0} b_r = 0. \tag{2.12}$$

For $m=1$, one finds

$$3i\frac{\partial}{\partial r}b_r + 2i\frac{\partial}{\partial z}b_z = k\cdot b_z. \tag{2.13}$$

In the limit $r\to 0$ we get homogeneous Neumann boundary condition

$$\lim_{r\to 0}\frac{\partial}{\partial r}b_r = 0. \tag{2.14}$$

2.2 Numerical implementation of Chebyshev spectral method

A classical Chebyshev spectral method based differential matrix [35, 36] is applied to solve bivariate Eqs. (2.6a) and (2.6b). First, we introduce the Chebyshev points

$$x_i = \frac{\cos \pi i}{N}, \quad i=0,\dots,N. \tag{2.15}$$

The entries of Chebyshev spectral differentiation matrix $\mathcal{D}_N$ are

$$d_{i,j} = \frac{c_i}{c_j}\frac{(-1)^{i+j}}{(x_i - x_j)}, \qquad 0\le i,j\le N, \quad i\neq j, \tag{2.16a}$$

$$d_{i,i} = -\frac{x_i}{2(1-x_i^2)}, \qquad 1\le i\le N-1, \tag{2.16b}$$

$$d_{0,0} = -d_{N,N} = \frac{2N^2+1}{6}, \tag{2.16c}$$

where $c_0=c_N=2$ and $c_j=1, 1\le j\le N-1$. Note that the diagonal entries $d_{i,i}$ can be evaluated better by

$$d_{i,i} = -\sum_{j=0, j\neq i}^{N} d_{i,j}, \tag{2.17}$$

to produce a matrix with better stability properties in the presence of rounding errors. The discrete derivative $U'(x_i)$ of a grid function $U(x_i)$ can be represented by multiplying Chebyshev differentiation matrix $\mathcal{D}_N$

$$U' = \mathcal{D}_N U. \tag{2.18}$$

Apparently, we can compute the second order derivative via $\mathcal{D}_N^2$, the square of $\mathcal{D}_N$.

For such a 2-D problem in the azimuthal plane, we naturally set up a tensor product grid based on Chebyshev points independently in each direction. Some notations we

adopt are presented as follows. Points $(r_0,r_1,\cdots,r_{N_r})$ are radial Chebyshev points rescaled to $[0,R_0]$ and $(Z_0,Z_1,\cdots,Z_{N_Z})$ are axial Chebyshev points rescaled to $[-1/2,1/2]$. $\mathcal{D}_r$ and $\mathcal{D}_z$ denote the radial and axial Chebyshev differentiation matrix also rescaled to $[0,R_0]$ and $[-1/2,1/2]$, respectively. The second order derivatives $\mathcal{D}_r^2$ and $\mathcal{D}_z^2$ are evaluated by squaring $\mathcal{D}_r$ and $\mathcal{D}_z$, respectively. I_r and I_z denote the $N_r\times N_r$ and $N_z\times N_z$ identity matrices, respectively, and $\mathcal{R}$ and $\widetilde{\mathcal{R}}$ are the diagonal matrices

$$\mathcal{R}=\text{Diag}(r_0,r_1,\cdots,r_N), \tag{2.19a}$$

$$\widetilde{\mathcal{R}}=\text{Diag}(1/r_0,1/r_1,\cdots,1/r_N). \tag{2.19b}$$

Note that $1/r_N$ has singularity since $r_N=0$ at axis $r=0$, an alternative way is to set $r_N=10^{-6}$ and the corresponding row and column of differential matrices will be deleted later due to the regularity condition.

Then the discretized matrices corresponding to bivariate Eqs. (2.6a) and (2.6b) are represented by the following Chebyshev differentiation matrix:

$$\mathbb{A}=-\frac{i}{m}(\mathcal{R}\otimes I_z)\cdot(\mathcal{D}_r\otimes I_z)\cdot(I_r\otimes\mathcal{D}_z)-\frac{i}{m}(I_r\otimes\mathcal{D}_z), \tag{2.20a}$$

$$\mathbb{B}=-\frac{i}{m}(\mathcal{R}\otimes I_Z)\cdot\left(I_r\otimes\mathcal{D}_Z^2\right)+im\left(\tilde{\mathcal{R}}\otimes I_Z\right), \tag{2.20b}$$

$$\mathbb{C}=\frac{i}{m}(\mathcal{R}\otimes I_z)\cdot\left(\mathcal{D}_r^2\otimes I_z\right)+\frac{3i}{m}(\mathcal{D}_r\otimes I_z)+\left(\frac{i}{m}-im\right)\left(\tilde{\mathcal{R}}\otimes I_z\right), \tag{2.20c}$$

$$\mathbb{D}=\frac{2i}{m}(I_r\otimes\mathcal{D}_z)+\frac{i}{m}(\mathcal{R}\otimes I_z)\cdot(\mathcal{D}_r\otimes I_z)\cdot(I_r\otimes\mathcal{D}_z), \tag{2.20d}$$

where the "$\cdot$" and "$\otimes$" denote the ordinary and the Kronecker product of two matrices, respectively. The operation for Kronecker product can be demonstrated by an example as

$$\begin{pmatrix}1&2\\3&4\end{pmatrix}\otimes\begin{pmatrix}a&b\\c&d\end{pmatrix}=\begin{pmatrix}a&b&2a&2b\\c&d&2c&2d\\3a&3b&4a&4b\\3c&3d&4c&4d\end{pmatrix}. \tag{2.21}$$

Now we define

$$\mathbb{M}\equiv\begin{pmatrix}\mathbb{A}&\mathbb{B}\\\mathbb{C}&\mathbb{D}\end{pmatrix}. \tag{2.22}$$

For $m>1$, the Eqs. (2.6a) and (2.6b) then become bivariate eigenvalue problem

$$\mathbb{M}\cdot\begin{pmatrix}\mathcal{B}_r\\\mathcal{B}_z\end{pmatrix}=k\begin{pmatrix}\mathcal{B}_r\\\mathcal{B}_z\end{pmatrix}. \tag{2.23}$$

For $m=1$, due to the homogeneous Neumann condition of b_r the equations become the following generalized eigenvalue problem

$$\mathbb{M}\cdot\begin{pmatrix}\mathcal{B}_r\\ \mathcal{B}_z\end{pmatrix}=k\mathbb{E}\cdot\begin{pmatrix}\mathcal{B}_r\\ \mathcal{B}_z\end{pmatrix}, \tag{2.24}$$

where $\mathbb{E}$ is the identity matrix with the same size as $\mathbb{M}$. The $\mathcal{B}_r$ and $\mathcal{B}_z$ are the radial and axial components of the helical $\boldsymbol{B}$ at 2-D Chebyshev collocation grids, i.e.,

$$\mathcal{B}_r=\left(B_r^{00},B_r^{10},\cdots,B_r^{N_z0},B_r^{01},B_r^{11},\cdots,B_r^{N_z1},\cdots,B_r^{N_zN_r}\right)^{\mathrm{T}}, \tag{2.25a}$$

$$\mathcal{B}_z=\left(B_z^{00},B_z^{10},\cdots,B_z^{N_z0},B_z^{01},B_z^{11},\cdots,B_z^{N_z1},\cdots,B_z^{N_zN_r}\right)^{\mathrm{T}}, \tag{2.25b}$$

where $\mathcal{B}_r^{ij}$ and $\mathcal{B}_z^{ij}$ represent $b_r\left(r_j,z_i\right)$ and $b_z\left(r_j,z_i\right)$, respectively.

The homogeneous Dirichlet boundary conditions imply that the corresponding rows and columns of $\mathbb{M}$ can be ignored. The corresponding index vector I can be obtained from the rows where the boundary points are located in a 1-D vector, which is stretched from the 2-D Chebyshev grids. Let $\widetilde{\mathbb{M}}$ denotes the modified matrix by stripping away the rows and columns of the index vector I. The modified vectors $\widetilde{\mathcal{B}}_r$ and $\widetilde{\mathcal{B}}_z$ are obtained by stripping the $\mathcal{B}_r$ and $\mathcal{B}_z$ of the corresponding rows. Therefore, for $m>1$, the modified eigenvalue problem becomes

$$\widetilde{\mathbb{M}}\cdot\begin{pmatrix}\widetilde{\mathcal{B}}_r\\ \widetilde{\mathcal{B}}_Z\end{pmatrix}=k\begin{pmatrix}\widetilde{\mathcal{B}}_r\\ \widetilde{\mathcal{B}}_z\end{pmatrix}. \tag{2.26}$$

For $m=1$, the modified matrix $\widehat{\mathbb{M}}$ is obtained by replacing the first $(N_r+1)\times(N_z+1)$ columns of the rows, which correspond to the points of b_r at the axis in $\mathbb{M}$, by the relevant rows of $\mathcal{D}_r\otimes I_z$, and the remaining columns are assigned to zero. Similarly, a modified matrix $\widehat{\mathbb{E}}$ is given by replacing the relevant rows of $\mathbb{E}$ with zero. Then, the Dirichlet boundary conditions are treated by the same way as for $m>1$ modes. The generalized eigenvalue problem is now

$$\widehat{\mathbb{M}}\cdot\begin{pmatrix}\widetilde{\mathcal{B}}_r\\ \widetilde{\mathcal{B}}_z\end{pmatrix}=k\hat{\mathbb{E}}\cdot\begin{pmatrix}\widetilde{\mathcal{B}}_r\\ \widetilde{\mathcal{B}}_z\end{pmatrix}. \tag{2.27}$$

For a dense matrix, a QZ algorithm is employed here to solve the above generalized eigenvalue problem in MATLAB ® 's built-in matrix eigenvalue routine eig.

With the b_r and b_z solved in Eqs. (2.26) and (2.27), the b_θ can be computed from the incompressible equation, i.e., Eq. (2.5). Let $\dot{\mathcal{B}}_r$ and $\dot{\mathcal{B}}_z$ be the 2-D matrix of the Chebyshev collocation grids, the matrix form of b_θ is

$$\dot{\mathcal{B}}_\theta=\frac{i}{m}\left(\dot{\mathcal{B}}_r+\dot{\mathcal{B}}_r\cdot\mathcal{D}_r^{\mathrm{T}}\cdot\mathcal{R}+\mathcal{D}_z\cdot\dot{\mathcal{B}}_z\cdot\mathcal{R}\right). \tag{2.28}$$

Note that the b_θ can also be calculated by Eq. (2.3b). However, such procedure will give rise to numerical oscillation at the corner nodes, whereas using the incompressible equation does not.

2.3 Symmetry property of the helical wave

A symmetry property of the helical wave in the circular cylindrical geometry should be presented. This property comes from the symmetry of geometry of 3-D domains, and it is very useful in the computation when the geometry of the considered domain is centrosymmetric.

First, there are at least two independent helical waves corresponding to the same eigenvalue k since both $b^m_{r,\theta,z}\cos(m\theta)$ and $b^m_{r,\theta,z}\sin(m\theta)$ are the eigenfunctions once the single helical mode is of the Fourier form $b^m_{r,\theta,z}e^{im\theta}$. This means there also exist two independent real helical wave for the same eigenvalue and thus the eigenvalue is duplicate at least. Second, due to the centrosymmetry of the cylindrical geometry, the positive and negative eigenvalues with the same absolute value appear in pairs for each m. And a pair of Fourier modes for $\pm|k|$ for each m to express the helical wave are correlated according to the following relations:

$$\text{for} \quad m>0, \quad \begin{cases} \boldsymbol{B}^m_{|k|} = \left(b^m_r, b^m_\theta, b^m_z\right) e^{im\theta} & \text{for eigenvalue } |k|, \\ \boldsymbol{B}^m_{-|k|} = \left(\left(b^m_r\right)^*, -\left(b^m_\theta\right)^*, \left(b^m_z\right)^*\right) e^{im\theta} & \text{for eigenvalue } -|k|, \end{cases} \tag{2.29a}$$

$$\text{for} \quad m<0, \quad \begin{cases} \boldsymbol{B}^m_{|k|} = \left((b^{|m|}_r)^*, (b^{|m|}_\theta)^*, (b^{|m|}_z)^*\right) e^{im\theta} & \text{for eigenvalue } |k|, \\ \boldsymbol{B}^m_{-|k|} = (b^{|m|}_r, -b^{|m|}_\theta, b^{|m|}_z) e^{im\theta} & \text{for eigenvalue } -|k|. \end{cases} \tag{2.29b}$$

Eq. (2.29b) is just a natural consequence that the superposition of helical wave

$$B_{r,\theta,z} = \sum_{m=-\infty}^{\infty} (\boldsymbol{B}^m_{\pm|k|})_{r,\theta,z} \tag{2.30}$$

are requested to be real vector field of 3-D space and therefore the conjugate relation between $b^m_{r,\theta,z}$ expressed by Eq. (2.2) appear automatically. This allows us to compute those eigenfunctions only for $m>0$.

Finally, it should be emphasized that all of these eigenfunctions satisfy the homogeneous boundary conditions due to the structure of Eq. (2.29a).

2.4 Criterion of spurious eigenvalue

In the background of our present work, the problem of spurious eigenvalues and eigenmodes should unavoidably be paid attention. Generally, spurious eigenvalues appear in numerical calculation of eigenvalue problem due to the under-resolution of genuine eigenmodes [38]. The typical method for removing spurious eigenvalues is to exclude nonconverging eigenvalues by repeating several calculations with different grids. Tang [33] has pointed out that the bivariate Eqs. (2.6a) and (2.6b) that explicitly enforce divergence-free condition for helical modes are less polluted by spurious modes than the primitive Eqs. (2.3a)-(2.3c). However, it is still a big challenge to lower the calculation

cost of removing spurious eigenvalues, because it is necessary to perform the calculation several times to determine whether the relative error converges, as illustrated by Tang [33].

In theory, the energy of the spurious eigenmodes is very low. However, we cannot judge such low-energy modes through the normalized numerical outputs of the standard matrix eigenvalue problem. There should be an alternative criterion to distinguish the spurious eigenmodes. Based on the fact that the spurious eigenmodes do not belong to the eigenfunction set of the curl operator, we find that an existing identity [39] that expresses the total energy of a Beltrami field in terms of a surface integral can just serve as a criterion of spurious eigenvalue. The identity reads

$$\int_{\mathcal{D}} B^2 dV = \int_{\partial\mathcal{D}} B^2 \boldsymbol{r}\cdot d\boldsymbol{S} - 2\int_{\partial\mathcal{D}} (\boldsymbol{B}\cdot\boldsymbol{r})(\boldsymbol{B}\cdot d\boldsymbol{S}), \tag{2.31}$$

where $B^2 = \boldsymbol{B}\cdot\boldsymbol{B}$ is the energy of the real helical wave, and $\boldsymbol{r}$ is the position vector starting from an arbitrary origin. For the helical wave with $\boldsymbol{B}\cdot d\boldsymbol{S} = 0$ as boundary condition, the identity reduces as

$$\int_{\mathcal{D}} B^2 dV = \int_{\partial\mathcal{D}} B^2 \boldsymbol{r}\cdot d\boldsymbol{S}. \tag{2.32}$$

In Appendix, we prove that this identity also holds for complex helical waves, if we give B^2 the meaning of $|\boldsymbol{B}|^2$.

The identity implies an important energy relation for any helical wave defined in a bounded 3-D domain, which is tangent to the boundary surface of the domain. The numerical criterion proposed to filter the spurious eigenmodes and the consequent spurious eigenvalues is defined by

$$\sigma \equiv \frac{\left|\int_{\mathcal{D}} B^2 dV - \int_{\partial\mathcal{D}} B^2 \boldsymbol{r}\cdot d\boldsymbol{S}\right|}{\int_{\mathcal{D}} B^2 dV} \geq \sigma_{\mathrm{C}}. \tag{2.33}$$

It can be proved that σ is actually controlled by a well-defined energy norm of the relative error of the computed helical waves, from which we obtained that

$$\sigma = \mathcal{O}(\max|\boldsymbol{B} - \boldsymbol{B}_0|). \tag{2.34}$$

Here, the $\boldsymbol{B}_0$ denotes the true or the approximated helical wave that has been normalized by the L^2 norm. All of the relevant details of the argumentation are supplied in the Appendix. It is expected that the spurious eigenmodes will give rise to a significant error norm and therefore the σ would exceed certain threshold σ_{C}. The determination of the σ_C depends on the accessible level of accuracy of the numerical computation, which is further relevant to the truncation error and the round error. A further argument and specific results will be presented in the next section.

To our best knowledge the criterion proposed is new. Moreover it can significantly reduce the calculation cost since the calculation is performed only once.

3 Numerical results

3.1 Convergence and accuracy of eigenfunctions and eigenvalues

Based on the Chebyshev spectral method formulated previously, a case demonstration is displayed. Here we take $R_0=0.25$, meaning that the ratio of height to diameter is 2. The convergence of the computed eigenvalues as a function of the number of grid points is shown in Table 1, wherein we take $N_z=4N_r$ since the height of the cylinder is 4 times the radius.

Table 1: The first 10 eigenvalues of helical modes at $m=3$.

Index	E. C. Morse [28]	$N_r=10$	$N_r=30$
1	24.6782477661218	24.6782509629646	24.6782477662102
2	25.5625440411167	25.5625475731572	25.5625440414496
3	26.8666453206450	26.8666514515229	26.8666453213065
4	28.4368538322556	28.4368695149927	28.4368538332641
5	30.1799718498448	30.1800052314483	30.1799718511973
6	32.0610758743960	32.0611308056641	32.0610758760922
7	34.0670197921808	34.0671007566754	34.0670197942201
8	36.1799016758825	36.1800249117142	36.1799016782458
9	37.7264135106135	37.7279550482058	37.7264135109012
10	38.2440896181714	38.2448688141708	38.2440896189689

The convergence of the residual of the computation represented by $\mathrm{Err}(b_\theta)$ defined in Eq. (3.1) (see also [33]), along with the relative error of the eigenvalue evaluated by $\mathrm{Err}(k)\equiv|k(N_r)-k(N_r=70)|/k(N_r=70)$ are shown in Fig. 1

$$\mathcal{R}(b_\theta)\equiv\frac{\partial b_r}{\partial z}-\frac{\partial b_z}{\partial r}-k\cdot b_\theta, \tag{3.1a}$$

$$\mathcal{M}(b_\theta)\equiv\frac{1}{2}\left(\frac{\partial b_r}{\partial z}-\frac{\partial b_z}{\partial r}+k\cdot b_\theta\right), \tag{3.1b}$$

$$\mathrm{Err}(b_\theta)\equiv\frac{\int\int\mathcal{R}^2(b_\theta)\cdot r dr dz}{\int\int\mathcal{M}^2(b_\theta)\cdot r dr dz}. \tag{3.1c}$$

The numerical result indicates that the residual is of $\mathcal{O}(N_r^{-4})$ for any helical wave with fixed label. This convergence rate lies in the fact that the Chebyshev expansion can be convergent algebraically on non-periodic domain like a cylinder with a finite length. The general result on the convergence rate is illustrated by Trefethen [35]. Compared with the finite difference method [33], the spectral method achieves a typical residual level of $\mathcal{O}(10^{-6})$ with much fewer grid points, under the considered scope of parameters. The level of the relative error of the computed eigenvalues is even smaller.

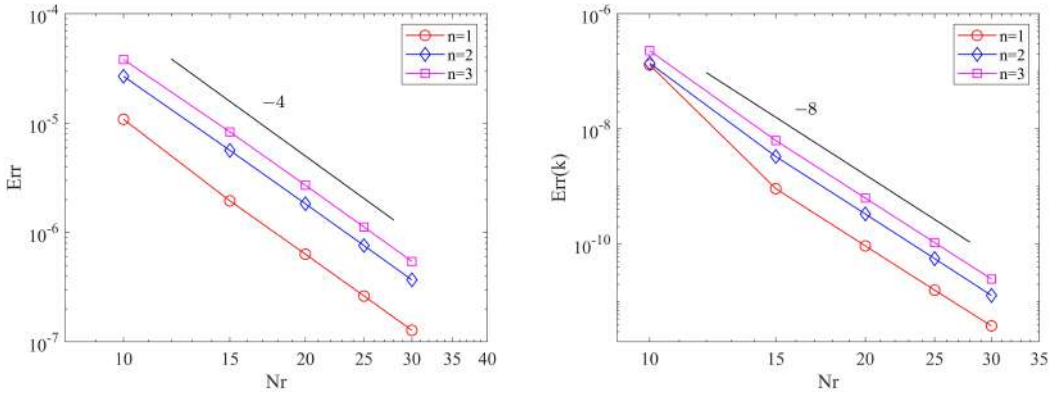

(a) $Err(b_\theta)$ are plotted as functions of Nr (b) $Err(k)$ are plotted as functions of Nr

Figure 1: The convergence of Err(b_θ) and Err(k) for the nth eigenvalue at $m=3$.

We know that helical waves of different eigenvalues are orthogonal. Therefore, the orthogonalization accuracy can be used to verify whether the number of the computation grid points are sufficient. The normalized coefficient c_n of helical wave is

$$c_n = \left(\int \boldsymbol{B} \cdot \boldsymbol{B}^* dV \right)^{-\frac{1}{2}} \tag{3.2}$$

and naturally the orthogonalization accuracy d_{12} can be measured in terms of

$$d_{12} = \int \boldsymbol{B}_1 \cdot \boldsymbol{B}_2^* dV, \tag{3.3}$$

where $\boldsymbol{B}_1$ and $\boldsymbol{B}_2$ denote the numerically normalized helical wave. The orthogonalization accuracies of the helical modes for $m=3$ are shown in Table 2.

Table 2: The orthogonalization accuracy of helical modes for $m=3$. $N_r=30$, $N_z=4N_r$.

(n_1,n_2)	(1,2)	(11,12)	(21,22)	(31,32)	(41,42)
$\lvert d_{12}\rvert$	6.11 E-08	5.68 E-06	2.13 E-05	2.72 E-05	5.57 E-06
(n_1,n_2)	(1,10)	(10,20)	(20,30)	(30,40)	(40,50)
$\lvert d_{12}\rvert$	1.77 E-07	9.07 E-07	8.75 E-07	3.02 E-06	2.79 E-05

3.2 Concerning spurious eigenvalues

It is observed that the volume integral and surface integral appearing in Eq. (2.32) exhibit remarkable difference in the numerical computation. For each eigenmode, the difference

Table 3: The volume and surface integral respect to "helical wave" corresponding to spurious eigenvalues.

m	eigenvalue	$\int B^2 dV$	$\int B^2 \boldsymbol{r}\cdot\boldsymbol{dS}$	σ
$10(N_r=10)$	9.66393058153239	5.9574873 E-4	3.7640344 E-1	630.82
	19.3175137923818	5.0778739 E-4	3.1910055 E-1	627.41
	28.9497792149881	4.0543541 E-4	2.5224011 E-1	621.14
$30(N_r=20)$	127.202125821719	1.5972880 E-5	3.1773984 E-2	1988.24
	135.063119832602	1.4861827 E-5	2.9380954 E-2	1975.94
	142.907983957222	1.3735205 E-5	2.7172541 E-2	1977.31
$60(N_r=30)$	240.575909639702	3.1375369 E-6	10866824 E-2	3462.49
	247.956276288191	3.0644213 E-6	1.0094055 E-2	3292.95
	254.325995435115	3.0623070 E-6	9.1608647 E-3	2990.49

Table 4: The volume and surface integrals respect to true helical waves.

m	eigenvalue	$\int B^2 dV$	$\int B^2 \boldsymbol{r}\cdot\boldsymbol{dS}$	σ
$10(N_r=10)$	57.7055869784940	1.4782495 E-3	1.5297180 E-3	3.48 E-2
	57.9775945702477	1.3259570 E-3	1.3679836 E-3	3.17 E-2
	58.4267240209706	1.2708831 E-3	1.3047569 E-3	2.67 E-2
$30(N_r=20)$	144.347641951720	3.0728171 E-4	3.0727466 E-4	2.29 E-5
	144.450847328404	2.7445460 E-4	2.7444754 E-4	2.57 E-5
	144.622684178780	2.6167061 E-4	2.6166256 E-4	3.07 E-5
$60(N_r=30)$	270.095938380067	1.1519272 E-4	1.1517933 E-4	1.16 E-4
	270.150836048074	1.0281925 E-4	1.0280731 E-4	1.16 E-4
	270.242307046357	9.7950790 E-5	9.7939413 E-5	1.16 E-4

is quantitatively measured by the normalized index σ as already introduced in Section 2.4. By this index the whole data set of numerical output falls into two categories: one with comparative small σ and the other with very large σ. The σ differs by several order of magnitudes between the two categories. Apparently the former correspond to the true eigenmodes and the latter are spurious eigenmodes with spurious eigenvalues. The dramatic gap of σ makes it easy to determine a threshold σ_C. The typical results are shown in Tables 3 and 4, wherein $\sigma_C = 0.1$ is taken and the results of the first three eigenvalues are listed for each m. Other choice of threshold, e.g., 0.2, 0.5 or even 1.0, is of course possible in our cases. However, we keep in mind that while this threshold serves to differ the two categories of eigenmodes effectively, it represents the tolerable level of the relative error of the computed eigenmode due to its implication as pointed in Section 2.4. In this sense, the value of 0.1 as the allowed maximal relative error seems reasonable.

As we can see from the Tables 3 and 4, the significant numerical differences between the volume integral and surface integral for spurious eigenvalues are due to the fact that the eigenfunctions are almost zero inside the cylinder with numerical oscillations near

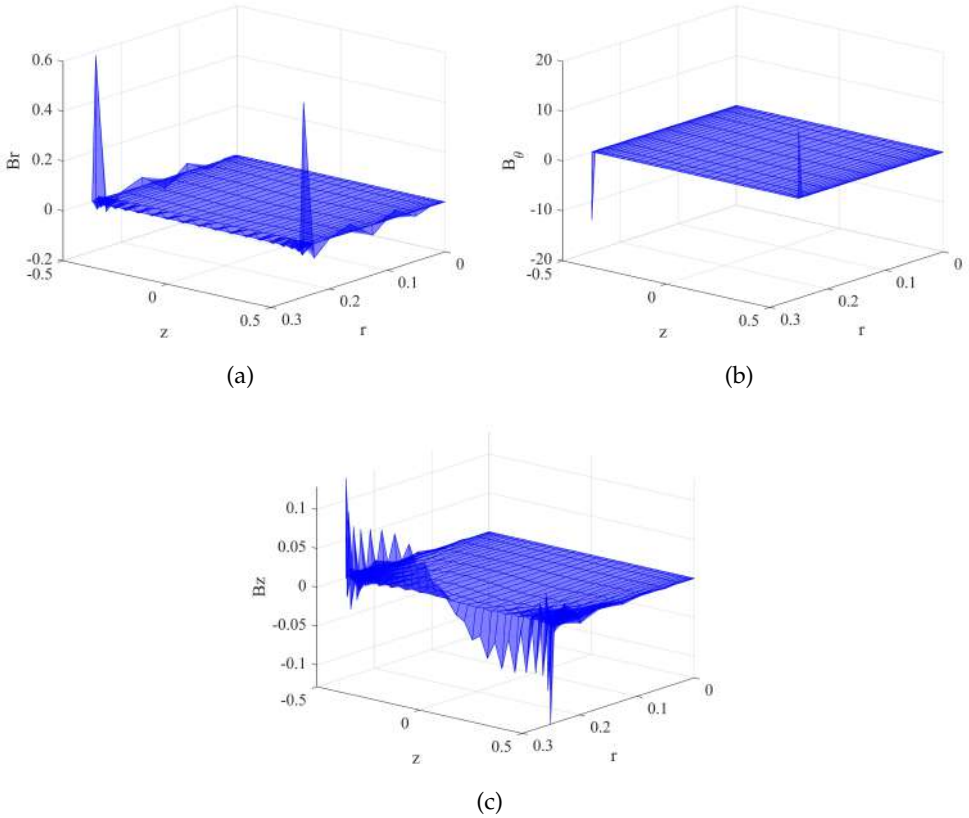

Figure 2: The imaginary part of b_r, b_θ, b_z for the first spurious eigenvalue for $m=3$. $N_r=10$, $N_z=4N_r$. The image of the real parts are similar to that of the imaginary parts.

the boundary, as shown in Fig. 2. Therefore, the surface integral is two or three orders of magnitudes larger than volume integral.

3.3 Configuration of the helical waves

Fig. 3 shows the streamlines for the real helical field corresponding to the lowest eigenvalue for $m=2$. While for axisymmetric helical waves each streamline lies on an axisymmetric torus, for non-axisymmetric helical waves concerned in this paper the streamlines can be chaotic since the global first integral for streamlines cannot be recognized any longer. Remind that chaotic streamlines is indeed the case for the superposition fields of two helical waves with the same eigenvalue but different orientation for spherical domains, as observed by Shi et al. [37]. The typical streamlines of helical waves we calculate in the finite cylinder are illustrated in Fig. 4, wherein only periodic and quasi-periodic streamlines are found. Meanwhile, it can be clearly seen as expected that the characteristic scale of the helical wave becomes smaller as the eigenvalue increases.

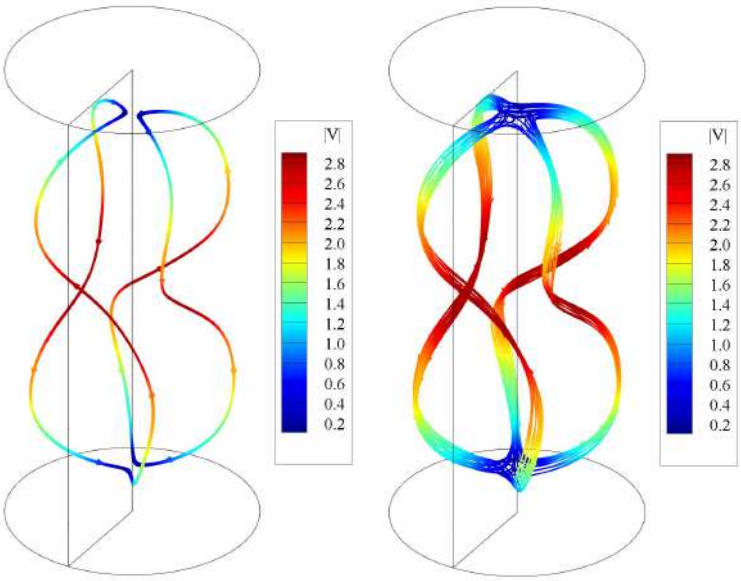

(a) a pair of periodic streamlines (b) a quasi-periodic streamline

Figure 3: Streamline of helical wave for the lowest eigenvalue for $m=2$.

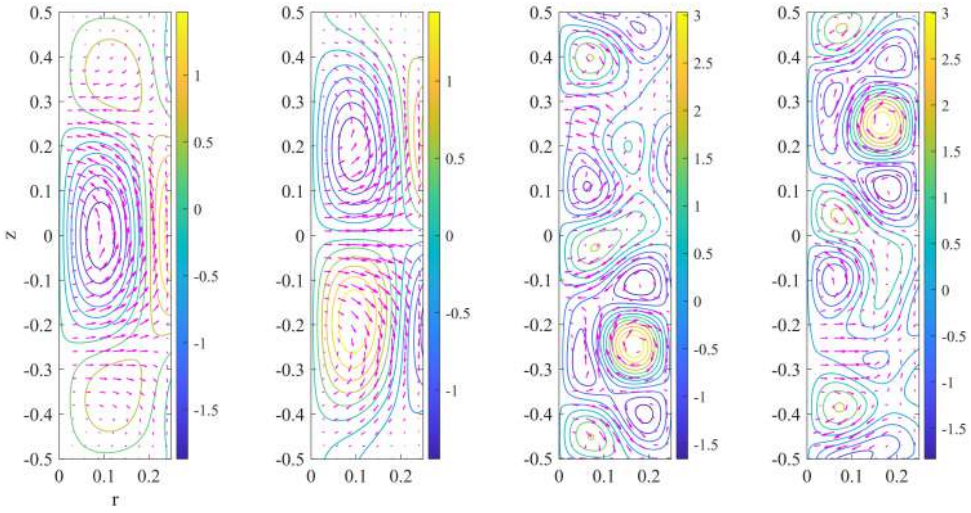

(a) (b) (c) (d)

Figure 4: Vector plot of (b_r,b_z) and contour plot of b_θ for the helical wave corresponding to the lowest eigenvalue and $10th$ eigenvalue for $m=2$ in the azimuthal plane of the finite circular cylinder. (a) The real part respect to the 1st eigenvalue; (b) the imaginary part respect to the 1st eigenvalue; (c) the real part respect to the 10th eigenvalue; (d) the imaginary part respect to the 10th of eigenvalue.

3.4 Asymptotic behavior of large eigenvalues

For larger eigenvalues, more grid points are required to resolve the finer scale of helical waves. The numerical tests show that the grid points of $N_r = 80$ are sufficient for the $m = 280$ helical modes, ensuring that the orthogonalization accuracies are around 10^{-5}. Additionally, the memory requirement of this grid is about 120GB in MATLAB ®. The eigenvalues of the $m = 280$ helical modes are shown in Table 5. The interval between these eigenvalues is much smaller than that in the $m = 2$ helical modes. Fig. 5 shows the contour plot of b_θ for the helical mode corresponding to the 30th eigenvalue for $m = 280$. Note that the components of $\boldsymbol{B}$ are small inside the cylinder while they are large near the boundary. However, since the maximal velocity is at the order $\mathcal{O}(1)$, the velocity of $\mathcal{O}(10^{-11})$ still remains within the double precision. It is straightforward to see that the azimuthal fields are similar to those represented by 2-D Fourier series. This asymptotic behavior of high wavenumber has also been illustrated by Su et al. [8].

It is important to investigate the asymptotic behavior in the limit $n \to \infty$, where n is the serial number of the discrete eigenvalues from small to large. Referring to Weyl theorem [40], the eigenvalues of the Laplace operator will tend to infinity as $\mathcal{O}(n^{2/3})$ in 3-D domains. For a sphere, the square of eigenvalues of the curl operator coincide

Table 5: The eigenvalues for helical mode for $m = 280$.

index	eigenvalue ($N_r = 60$)	eigenvalue ($N_r = 80$)
1	1169.19080378001	1169.19080378088
2	1169.20346684213	1169.20346684299
3	1169.22457164063	1169.22457164143
4	1169.25411771796	1169.25411771867
5	1169.29210443364	1169.29210443424
6	1169.33853096425	1169.33853096471
7	1169.39339630374	1169.39339630403
8	1169.45669926318	1169.45669926328
9	1169.52843847123	1169.52843847115
10	1169.60861237412	1169.60861237378
201	1231.45967916162	1231.45967912746
202	1232.08535801264	1232.08535797005
203	1232.38065411391	1232.38065394132
204	1232.72250241083	1232.72250236704
205	1233.36621791279	1233.36621791828
206	1233.37764891913	1233.37764869176
207	1234.01927755101	1234.01927750852
208	1234.38012375685	1234.38012357206
209	1234.67945747190	1234.67945742790
210	1235.34150332264	1235.34150324872

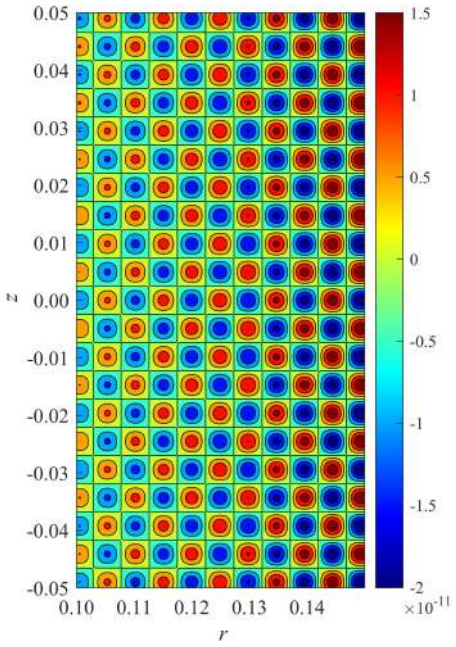

Figure 5: The contour plot of b_θ for the $30th$ eigenvalue for $m=280$ in the partial $[r,z]$ region of $[0.1,0.15]\times[-0.05,0.05]$.

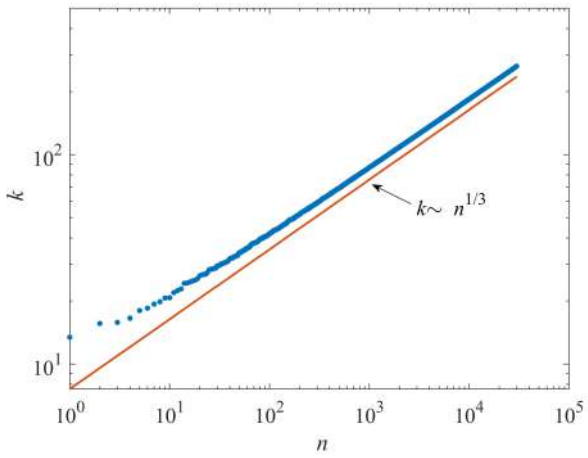

Figure 6: The distribution of positive eigenvalues in a finite circular cylinder with serial number n.

precisely with those of the Laplacian under homogeneous Dirichlet boundary condition. Here, we find that the eigenvalues of curl operator in the finite cylinder also obey the power law of $n^{1/3}$, as shown in Fig. 6, where only positive eigenvalues are plotted. It can

be verified that the eigenvalues of the curl operator for finite circular cylinder coincide with those of the Laplacian only for axisymmetric modes corresponding to $m=0$. For the Laplacian under homogeneous Dirichlet boundary condition, the eigenvalue sequence is formulated as

$$\lambda^2_{m,q,n}=(n\pi/h)^2+(\mu_{m,q}/R_0)^2,\quad m=0,1,2,\ldots,\quad n=1,2,\ldots,\quad q=1,2,\ldots, \tag{3.4}$$

where $\mu_{m,q}$ is the q-th zero of Bessel function $J_m(r)$ and h is the height of the cylinder. Hence the square root of the first five eigenvalues for $m=3$, $h=1.0$, $R_0=0.25$, say, are evaluated and ranked as

$$25.7133\ldots,\quad 26.2827\ldots,\quad 27.2053\ldots,\quad 28.4467\ldots,\quad 29.9674\ldots. \tag{3.5}$$

Apparently the sequence is not the same as what has been listed in Table 1, showing the difference on eigenvalues for $m\neq 0$ between the curl operator and the Laplace operator.

4 Summary

In this paper, the non-axisymmetric helical waves in a finite circular cylinder are numerically computed via a Chebyshev spectral method as well as a new criterion proposed to rule out the spurious eigenvalues. The method is implemented by a Chebyshev differentiation matrix. Compared with the existing work, high wavenumber modes can be resolved in the present study due to the high accuracy the algorithm can accesses. This is a requisite for turbulence research in arbitrary bounded domains by means of HWD, which is the natural generalization of Fourier expansion used as a pivotal tools for turbulence in periodic box.

We first review the Chandrasekhar-Kendall modes generated by a scalar Helmholtz equation for bounded domains. Due to the coupling variables in radial and axial direction for a cylinder, Morse has found the non-axisymmetric CK modes represented by a series solution in terms of radial Bessel functions. The eigenvalues generated by this semi-analytical solution have high precision. However, the completeness of helical waves is lost in double precision calculation since Bessel functions at small variable with high m modes are too small to be represented within the machine precision. In addition, we correct the eigenvalue equation appeared in [28].

To solve the helical waves in high precision, Chebyshev spectral method is employed to discretize the two component equations presented by Tang [33]. The differentiation matrix is formed on 2-D spectral collocation grid points in the meridian plane of the cylinder. The regularity conditions at axis are then derived in detail. The numerical implementation of the Chebyshev spectral method and the convergence of eigenfunctions with the finer grids are presented. Also the orthogonalization accuracy of helical waves with large eigenvalues is presented. Furthermore, the distribution of the eigenvalues and the asymptotic behavior are demonstrated. It is found that the square of eigenvalues for non-axisymmetric helical waves is distinct from those of the Laplacian, though the

two sets of eigenvalues are identical for the axisymmetric modes, once the square of the eigenvalues of the curl operator are used instead of the signed ones.

To remove spurious eigenvalues, several calculations with different grids are always taken. This will cause high calculation costs. We find a new criterion based on an energy identity for helical modes. Thus, the calculation can be performed only once and the computation cost is significantly reduced.

Appendix

We now prove the crucial identity, i.e., Eq. (2.32) for any helical wave tangential to the boundary surface and allowing complex number representation. Then the essence of the criterion proposed for ruling out spurious eigenmodes and eigenvalues during the computation, i.e., Eq. (2.33), can be demonstrated.

For an arbitrary solenoidal vector field $\boldsymbol{B}$ with a form of complex number, which is defined in three-dimensional domain $\mathcal{D}$ and tangent to the boundary $\partial\mathcal{D}$, there holds

$$\begin{aligned}\int_{\mathcal{D}} \boldsymbol{r}\cdot(\nabla\times\boldsymbol{B})\times\boldsymbol{B}^* dV &= \int_{\mathcal{D}} (\nabla\times\boldsymbol{B})\cdot(\boldsymbol{B}^*\times\boldsymbol{r})\cdot\boldsymbol{dS}\\ &= \int_{\mathcal{D}} \boldsymbol{B}\cdot\nabla\times(\boldsymbol{B}^*\times\boldsymbol{r})dV+\int_{\partial\mathcal{D}}\boldsymbol{B}\times(\boldsymbol{B}^*\times\boldsymbol{r})\cdot\boldsymbol{dS}\\ &= \int_{\mathcal{D}} \boldsymbol{B}\cdot(\boldsymbol{r}\cdot\nabla\boldsymbol{B}^*+2\boldsymbol{B}^*)dV-\int_{\partial\mathcal{D}}(\boldsymbol{B}\cdot\boldsymbol{B}^*)\boldsymbol{r}\cdot\boldsymbol{dS},\end{aligned} \tag{A.1}$$

where $\boldsymbol{r}$ is the position vector and the superscript "$*$" denotes the complex conjugate. Taking the complex conjugate of the identity, we have

$$\int_{\mathcal{D}} \boldsymbol{r}\cdot(\nabla\times\boldsymbol{B}^*)\times\boldsymbol{B}dV = \int_{\mathcal{D}} \boldsymbol{B}^*\cdot(\boldsymbol{r}\cdot\nabla\boldsymbol{B}+2\boldsymbol{B})dV-\int_{\partial\mathcal{D}}(\boldsymbol{B}^*\cdot\boldsymbol{B})\boldsymbol{r}\cdot\boldsymbol{dS}. \tag{A.2}$$

For any helical wave $\boldsymbol{B}$, satisfying the properties

$$\nabla\times\boldsymbol{B}=k\boldsymbol{B},\quad \nabla\times\boldsymbol{B}^*=k\boldsymbol{B}^*, \tag{A.3}$$

and the non-penetration boundary conditions, i.e., $\boldsymbol{B}\cdot\boldsymbol{n}=\boldsymbol{B}^*\cdot\boldsymbol{n}=0$, the above identities read

$$k\int_{\mathcal{D}} \boldsymbol{r}\cdot\boldsymbol{B}\times\boldsymbol{B}^* dV = \int_{\mathcal{D}} \boldsymbol{B}\cdot(\boldsymbol{r}\cdot\nabla\boldsymbol{B}^*+2\boldsymbol{B}^*)dV-\int_{\partial\mathcal{D}}(\boldsymbol{B}\cdot\boldsymbol{B}^*)\boldsymbol{r}\cdot\boldsymbol{dS}, \tag{A.4a}$$

$$k\int_{\mathcal{D}} \boldsymbol{r}\cdot\boldsymbol{B}^*\times\boldsymbol{B}dV = \int_{\mathcal{D}} \boldsymbol{B}^*\cdot(\boldsymbol{r}\cdot\nabla\boldsymbol{B}+2\boldsymbol{B})dV-\int_{\partial\mathcal{D}}(\boldsymbol{B}^*\cdot\boldsymbol{B})\boldsymbol{r}\cdot\boldsymbol{dS}. \tag{A.4b}$$

Taking the summation of the two equations gives

$$0=\int_{\mathcal{D}} \boldsymbol{r}\cdot\nabla(\boldsymbol{B}\cdot\boldsymbol{B}^*)dV+4\int_{\mathcal{D}}\boldsymbol{B}\cdot\boldsymbol{B}^*dV-2\int_{\partial\mathcal{D}}(\boldsymbol{B}\cdot\boldsymbol{B}^*)\boldsymbol{r}\cdot\boldsymbol{dS}. \tag{A.5}$$

Substituting

$$\int_{\mathcal{D}} \boldsymbol{r}\cdot\nabla(\boldsymbol{B}\cdot\boldsymbol{B}^*)dV=\int_{\partial\mathcal{D}}(\boldsymbol{B}\cdot\boldsymbol{B}^*)\boldsymbol{r}\cdot\boldsymbol{dS}-3\int_{\mathcal{D}}\boldsymbol{B}\cdot\boldsymbol{B}^*dV \tag{A.6}$$

and $\boldsymbol{B}\cdot\boldsymbol{B}^*=|\boldsymbol{B}|^2$, we arrive at the following "energy" identity

$$\int_{\mathcal{D}}|\boldsymbol{B}|^2dV-\int_{\partial\mathcal{D}}|\boldsymbol{B}|^2\boldsymbol{r}\cdot\boldsymbol{dS}=0. \tag{A.7}$$

We now take into account the influence of the computation error. Return to arbitrary solenoidal vector field $\boldsymbol{B}$ defined in $\mathcal{D}$ and tangent to $\partial\mathcal{D}$. Taking the summation of Eq. (A.1) and Eq. (A.2) again and using Eq. (A.6), we obtain

$$\int_{\mathcal{D}}\boldsymbol{r}\cdot(\nabla\times\boldsymbol{B})\times\boldsymbol{B}^*dV+\int_{\mathcal{D}}\boldsymbol{r}\cdot(\nabla\times\boldsymbol{B}^*)\times\boldsymbol{B}dV=\int_{\mathcal{D}}|\boldsymbol{B}|^2dV-\int_{\partial\mathcal{D}}|\boldsymbol{B}|^2\boldsymbol{r}\cdot\boldsymbol{dS}. \tag{A.8}$$

Define that

$$D_b\equiv\int_{\mathcal{D}}|\boldsymbol{B}|^2dV-\int_{\partial\mathcal{D}}|\boldsymbol{B}|^2\boldsymbol{r}\cdot\boldsymbol{dS} \tag{A.9}$$

and rewrite Eq. (A.8) as

$$D_b=\int_{\mathcal{D}}\boldsymbol{r}\cdot(\nabla\times\boldsymbol{B}-k\boldsymbol{B})\times\boldsymbol{B}^*dV+\int_{\mathcal{D}}\boldsymbol{r}\cdot(\nabla\times\boldsymbol{B}^*-k\boldsymbol{B}^*)\times\boldsymbol{B}dV, \tag{A.10}$$

then using the Cauchy-Schwarz inequality we have the following estimation that

$$|D_b|\leq 2L\left(\int_{\mathcal{D}}|\nabla\times\boldsymbol{B}-k\boldsymbol{B}|^2dV\right)^{\frac{1}{2}}\left(\int_{\mathcal{D}}|\boldsymbol{B}|^2dV\right)^{\frac{1}{2}}, \tag{A.11}$$

where L is the maximum of $|\boldsymbol{r}|$ within $\mathcal{D}$. If we introduce the L^2 norm $\|\cdot\|_2$ of a vector field defined in $\mathcal{D}$, then Eq. (A.11) can be expressed as

$$|D_b|\leq 2L\|\nabla\times\boldsymbol{B}-k\boldsymbol{B}\|_2\cdot\|\boldsymbol{B}\|_2. \tag{A.12}$$

When $\boldsymbol{B}$ is considered as the approximate helical wave by numerical computation, the approximation error can be measured by a relative residual defined as

$$\mathrm{Err}(\boldsymbol{B})\equiv\frac{\|\nabla\times\boldsymbol{B}-k\boldsymbol{B}\|_2^2}{\|(\nabla\times\boldsymbol{B}+k\boldsymbol{B})/2\|_2^2}\approx\frac{\|\nabla\times\boldsymbol{B}-k\boldsymbol{B}\|_2^2}{k^2\|\boldsymbol{B}\|_2^2}. \tag{A.13}$$

If we define a dimensionless index as

$$\sigma\equiv\frac{|D_b|}{\|\boldsymbol{B}\|_2^2} \tag{A.14}$$

and denote the difference between the true helical wave $\boldsymbol{B}_0$ and the approximated one by $\boldsymbol{b}$, then there will be

$$\sigma \leq 2Lk\sqrt{\mathrm{Err}(\boldsymbol{B})} \leq 2\sqrt{2}L\left(\|\nabla\times\boldsymbol{b}\|_2^2+k^2\|\boldsymbol{b}\|_2^2\right)^{\frac{1}{2}}/\|\boldsymbol{B}\|_2. \tag{A.15}$$

This inequality indicates the relation between σ and the relative error function defined in the text, thus it is necessary for the clarity. However, the estimation is rather loose because the wavenumber k as the prefactor appearing in the inequality can be large. A better estimation can be realized by substituting the expression $\boldsymbol{B}=\boldsymbol{B}_0+\boldsymbol{b}$ straightforwardly into Eq. (A.9) and simplifying. Following this line we obtain

$$D_b = 2\int_{\mathcal{D}} \boldsymbol{B}_0\cdot\boldsymbol{b}dV+\int_{\mathcal{D}}|\boldsymbol{b}|^2dV+2\int_{\partial\mathcal{D}}(\boldsymbol{B}_0\cdot\boldsymbol{b})\boldsymbol{r}\cdot\boldsymbol{dS}+2\int_{\partial\mathcal{D}}|\boldsymbol{b}|^2\boldsymbol{r}\cdot\boldsymbol{dS}. \tag{A.16}$$

If the centre of the cylinder is chosen as the original, then we have $0<\boldsymbol{r}\cdot\boldsymbol{dS}=r\cdot dS\leq L\cdot dS$ with L being the maximum of $|\boldsymbol{r}|$. Using the Cauchy-Schwarz inequality again, we have

$$\int_{\mathcal{D}}\boldsymbol{B}_0\cdot\boldsymbol{b}dV\leq\|\boldsymbol{B}_0\|_2\cdot\|\boldsymbol{b}\|_2, \tag{A.17a}$$

$$\int_{\partial\mathcal{D}}(\boldsymbol{B}_0\cdot\boldsymbol{b})\boldsymbol{r}\cdot\boldsymbol{dS}\leq\left(\int_{\partial\mathcal{D}}|\boldsymbol{B}_0|^2\boldsymbol{r}\cdot\boldsymbol{dS}\right)^{\frac{1}{2}}\left(\int_{\partial\mathcal{D}}|\boldsymbol{b}|^2\boldsymbol{r}\cdot\boldsymbol{dS}\right)^{\frac{1}{2}}. \tag{A.17b}$$

Since $\boldsymbol{B}_0$ is a normalized helical wave, there is

$$\int_{\partial\mathcal{D}}|\boldsymbol{B}_0|^2\boldsymbol{r}\cdot\boldsymbol{dS}=\int_{\mathcal{D}}|\boldsymbol{B}_0|^2dV=\|\boldsymbol{B}_0\|_2^2=1. \tag{A.18}$$

Then Eq. (A.17b) means

$$\int_{\partial\mathcal{D}}(\boldsymbol{B}_0\cdot\boldsymbol{b})\boldsymbol{r}\cdot\boldsymbol{dS}\leq\sqrt{L}\left(\int_{\partial\mathcal{D}}|\boldsymbol{b}|^2dS\right)^{\frac{1}{2}}. \tag{A.19}$$

And finally the estimation of σ can be given as

$$\sigma=\mathcal{O}\left(2\|\boldsymbol{b}\|_2+2\sqrt{L}\left(\int_{\partial\mathcal{D}}|\boldsymbol{b}|^2dS\right)^{\frac{1}{2}}\right)=\mathcal{O}(\max|\boldsymbol{b}|). \tag{A.20}$$

Here, the second order terms have been neglected due to the smallness of $|\boldsymbol{b}|$ and $\sigma\approx D_b$ is taken into account. Because $\boldsymbol{b}$ is also normalized by $\|\boldsymbol{B}_0\|_2$, the estimation indicates that the index σ is actually an equivalent measurement for the **relative error** of computed helical wave. If σ exceeds certain prescribed threshold σ_C, then the numerical approximation to the true helical wave is worse. Therefore, $\sigma\leq\sigma_C$ with σ expressed by Eq. (A.14) along with an appropriate σ_C can be a criterion to remove the spurious eigenmodes and the parallel spurious eigenvalues.

Acknowledgements

The first author thanks Dr. Ankang Gao for helpful discussions. We are indebted to Prof. E. C. Morse for his generous help in the early stage of the study. The anonymous reviewers are highly appreciated for their very enlightening and constructive comments. This work was supported by the National Natural Science Foundation of China (No. 11672005).

References

[1] E. Beltrami, *Considerazioni idrodinamiche,* Il Nuovo Cimento, 25 (1899), pp. 212–222.
[2] L. Woltjer, *A theorem on force-free magnetic fields,* Proc. Nat. Acad. Sci., 44 (1958), pp. 489–491.
[3] J. B. Taylor, *Relaxation of toroidal plasma and generation of reverse magnetic fields,* Phys. Rev. Lett., 33 (1974), pp. 1139–1141.
[4] P. Constantin and A. Majda, *The Beltrami spectrum for incompressible fluid flows,* Commun. Math. Phys., 115 (1988), pp. 435–456.
[5] F. Waleffe, *The nature of triad interactions in homogeneous turbulence,* Phys. Fluids A, 4 (1992), pp. 350–363.
[6] H. K. Moffatt, *Dynamo action associated with random inertial waves in a rotating conducting fluid,* J. Fluid Mech., 44 (1970), pp. 705–719.
[7] Z. Yoshida and Y. Giga, *Remarks on spectra of operator rot,* Math. Z., 204 (1990), pp. 235–245
[8] Z.-J. Liao and W.-D. Su, *Kolmogorov's hypotheses and global energy spectrum of turbulence,* Phys. Fluids, 27 (2015), 041701.
[9] F. Waleffe, *Inertial transfers in the helical decomposition,* Phys. Fluids A Fluid Dyn., 5 (1993), pp. 677–685.
[10] Q. N. Chen, S. Y. Chen and G. L. Eyink, *The joint cascade of energy and helicity in three-dimensional turbulence,* Phys. Fluids, 15 (2003), pp. 361–374.
[11] L. Biferale, S. Musacchio and F. Toshi, *Inverse energy cascade in three-dimensional isotropic turbulence,* Phys. Rev. Lett., 108 (2012), 164501.
[12] Ibid, *Split energy-helicity cascades in three-dimensional homogeneous and isotropic turbulence,* J. Fluid Mech., 730 (2013), pp. 309–327.
[13] L. M. Smith and Y. Lee, *On near resonances and symmetry breaking in forced rotating flows at moderate Rossby number,* J. Fluid Mech., 535 (2005), pp. 111–142.
[14] L. Bourouiba and P. Bartello, *The intermediate Rossby number range and two-dimensional-three-dimensional transfers in rotating decaying homogeneous turbulence,* J. Fluid Mech., 587 (2007), pp. 139–161.
[15] J. B. Taylor, *Relaxation and magnetic reconnection in plasmas,* Rev. Mod. Phys, 58 (1986), pp. 741–763.
[16] X. Z. Tang and A. H. Boozer, *Force-free magnetic relaxation in driven plasmas,* Phys. Rev. Lett., 94 (2005), 225004.
[17] X. W. Shan, D. C. Montgomery and H. D. Chen, *Nonlinear magnetohydrodynamics by Galerkin-method computation,* Phys. Rev. A, 44 (1991), pp. 6800–6818.
[18] D. D. Hua, T. K. Fowler and E. C. Morse, *Magnetic relaxation in spheromaks using spectral expansions in cylindrical geometry,* J. Plasma Phys., 66 (2001), pp. 275–294.

[19] P. D. MININNI AND D. C. MONTGOMERY, *Magnetohydrodynamic activity inside a sphere,* Phys. Fluids, 18 (2006), 116602.
[20] P. D. MININNI, D. C. MONTGOMERY AND L. TURNER, *Hydrodynamic and magnetohydrodynamic computations inside a rotating sphere,* New J. Phys, 9 (2007), 303.
[21] Z.-J. LIAO AND W.-D. SU, *A Galerkin spectral method based on helical-wave decomposition for the incompressible Navier-Stokes equations,* Int. J. Numer. Meth. Fluids, 78 (2015), pp. 140–161.
[22] W.-D. SU AND Y. TAN, *Stream helicity in toroidal domains,* Adv. Appl. Math. Mech., 11 (2009), pp. 619–629.
[23] O. BOGOYAVLENSKIJ, *Vortex knots for the spheromak fluid flow and their moduli spaces,* J. Math. Anal. Appl., 450 (2017), pp. 21–47.
[24] H. E. MOSES, *Eigenfunctions of the curl operator, rotationally invariant Helmholtz theorem, and applications to electromagnetic theory and fluid mechanics,* SIAM J. Appl. Math., 21 (1971), pp. 114–144.
[25] J. CANTARELLA,D. DETURCK, H. GLUCK AND M. TEYTEL, *The spectrum of the curl operator on spherically symmetric domains,* Phys. Plasmas, 7 (2000), pp. 2766–2775.
[26] S. CHANDRASEKHAR AND P. C. KENDALL, *On force-free magnetic fields,* Astrophy. J, 126 (1957), pp. 457–460.
[27] L. TURNER, *Analytic solutions of $\nabla\times B=\lambda B$ having separatrices for geometries with one ignorable coordinate,* Phys. Fluids, 27 (1984), pp. 1677–1685.
[28] E. C. MORSE, *Eigenfunctions of the curl in cylindrical geometry,* J. Math. Phys., 46 (2005), 113511.
[29] IBID, *Eigenfunctions of the curl in annular cylindrical and rectangular geometry,* J. Math. Phys., 48 (2007), 083504.
[30] Y.-T. YANG, W.-D. SU AND J.-Z. WU, *Helical-wave decomposition and applications to channel turbulence with streamwise rotation,* J. Fluid Mech., 662 (2010), pp. 91–122.
[31] G. ALKAUSKAS, *Beltrami vector fields with an icosahedral symmetry,* J. Geometry Phys., 153 (2020), pp. 1–14.
[32] T. Z. BOULMEZAOUD AND T. AMARI, *Approximation of linear force-free fields in bounded 3-D domains,* Math. Comput. Model., 31 (2000), pp. 109–129.
[33] X. Z. TANG, *Numerical computation of the helical Chandrasekhar-Kendall modes,* J. Comput. Phys., 230 (2011), pp. 907–919.
[34] J. M. FINN, W. M. MANHEIMER AND E. OTT, *Spheromak tilting instability in cylindrical geometry,* Phys. Fluids, 24 (1981), pp. 1336–1341.
[35] L. N. TREFETHEN, Spectral Methods in Matlab, Society for Industrial and Applied Mathematics, 2000.
[36] R. PEYRET, Spectral Methods for Incompressible Viscous Flow, Springer Science & Business Media, 2002.
[37] C.-C. SHI, Y.-N. HUANG, Z.-X. ZHU, W.-D. SU AND Y.-F. DONG, *Chaotic phenomena produced by the spherical vortices in the Beltrami flows,* Chinese Phys. Lett., 9 (1992), pp. 515–518.
[38] J. P. BOYD, Chebyshev and Fourier Spectral Methods, Second edition, Courier Dover Publications, 2001.
[39] S. CHANDRASEKHAR, Hydrodynamic and Hydromagnetic Stability, Oxford University Press, 1961.
[40] R. COURANT AND D. HILBERT, Methods of Mathematical Physics (Vol. I), Interscience Publishers, New York, 1953.